SiC nanowires: material and devices

K. Zekentes, K Rogdakis

SiC nanowires: material and devices

K Zekentes and K Rogdakis

Institute of Electronic Structure & Laser, Foundation for Research and Technology-Hellas, Vassilika Vouton, 70013 Heraklion, Greece

Abstract. SiC nanowires are of high interest since they combine the physical properties of SiC with those induced by their low dimensionality. For this reason, a large number of scientific studies have been dedicated to their fabrication and characterization as well as to their application in devices. SiC nanowires growth involving different growth mechanisms and configurations was the main theme for the large majority of these studies. Various physical characterization methods have been employed for evaluating SiC nanowire quality. Very low diameter (<10 nm) nanowires as well as nanowires free of planar defects have not been demonstrated and these are some of the main challenges. Another issue is the high unintentional doping of the nanowires that does not allow the demonstration of high performance field effect transistors using SiC nanowires as channel material. On the other hand, the grown nanowires are suitable for field emission applications and to be used as reinforcing material in composite structures as well as for increasing the hydrophobicity of Si surfaces. All these aspects are examined in detail in the different sections of the present paper.

1. Introduction

In the recent years, the nanotechnology has become increasingly mature following an intense effort of material scientists, physicists, chemists, and engineers who have been inspired by its importance in both basic research and technological applications. The borders between physics, chemistry, materials science, biology etc, become undistinguishable on the nanometre scale. Thus, any breakthrough could have an impact on these areas, and already had.

This is the case in nanoelectronics. Indeed, the related semiconductor research has been the most important driving force behind nanotechnology. The reason is that one can achieve a maximum degree of control of the semiconductor material dimensions by very advanced lithography techniques. For instance, one-dimensional (1D) structures can function both as active components of devices (e.g. the channel in field-effect transistor (FET)) as well as interconnects and thus have the potential to provide two of the most critical functions in any integrated nanoelectronic system.

The 1D structures include nanotubes (hollow in the center), nanowires (solid in the center), nanorods (low length to diameter ratio nanowires; usually up to 10:1) and nanocables (coaxial 1D structures having a nanowire core material covered by a different outer material).

Among these different nanostructures, nanowires (NWs) have been most investigated because they are considered as a suitable solution for overcoming the fundamental limitations of planar MOSFET devices in downscaling [1]. The nanowire (NW) approach allows, indeed, for a coaxial gate-dielectric channel geometry that offers superior electrostatic control and consequently allowing continued scaling beyond what is possible with planar technology. Moreover, the 1D-character of carrier transport implies a reduced phase space for scattering of the carriers and opens up the possibility of ballistic transport. Finally, power dissipation is low and enhanced carrier mobility values are anticipated. The low and with energy-decreasing 1D density of states (DOS) allows reaching the quantum capacitance limit [2].

Except for employing nanowires for high-performance logic applications, where they act as active channel or interconnects, many other applications can take profit from their 1D character. Quantum mechanical effects, such as tunneling and electron wave interference, allow us to invent very sensitive and high-performance optoelectronic devices [3]. The surface to volume ratio becomes so large that the thermodynamic properties would change resulting in new devices like sensors with outstanding performance [4]. The nanoscale confinement of the channel current of a nanowire FET (NWFET), in concert with the large-surface area-to-volume ratio, enables charged molecules bound to the surface to effectively gate the device. This functionalization of the NW surface with specific receptors allows direct electronic detection of particular molecules of interest [4]. NWs are also very promising for field-emission-cathode applications since they present an extremely high aspect ratio, an important characteristic for this application.

Silicon carbide (SiC) is widely investigated [5] due to its physical properties like the: wide bandgap high thermal conductivity, high breakdown electric field, high electron drift velocity, high Young's modulus and hardness, high melting temperature, excellent oxidation and corrosion durability, high strength at elevated temperatures, good thermal shock resistance and excellent chemical and physical stability. The native oxide is silicon dioxide, which makes SiC directly compatible with usual Si technology.

SiC NWs combine the above properties of 1D materials with that of SiC and devices based on SiC nanowires are expected to present concrete advantages. Indeed, SiC NWs have been extensively studied in recent years because of their unique electronic [6], field-emitting [7], hydrophobic [8] and mechanical properties [9] and their potential applications in areas such as electronic and optoelectronic nanodevices, nanocomposites and hydrophobic devices.

For instance, SiC nanowire field effect transistors (SiC-NWFETs) are expected to be able to operate at temperatures higher than their Si-based counterparts. Indeed, a problem of Si NWFETs is the limited range of high temperature operation and for this reason the ITRS 2009 set as a target an operation tolerance up to 100ºC for nanodevices [10]. On the other hand, scaling has led to increasing power dissipation that result in higher chip temperatures, larger temperature cycles, and increased thermal gradients, all of which impact multiple failure mechanisms. The temperature effects are further aggravated by the reduced thermal conductivity in parallel to the reduction in the dielectric constant of the dielectrics between metal lines [10]. As a consequence, the materials and processes on which the computer revolution has been built are beginning to hit fundamental physical limits. Indeed, the synergic effects of the increased thermal noise, heat dissipation and bandwidth during miniaturization are manifest themselves in either a high bit-error rate or chip overheating [11]. So, the anticipated high temperature operation of SiC NWFETS is an important advantage for this type of application.

SiC NWs also present concrete advantages for forming field emission cathodes since apart their high aspect ratio, they present low electron affinity value and excellent chemical and physical stability [12]. Finally, SiC NWs are very attractive for thermoelectric applications due to, from one hand, the excellent thermoelectric properties of bulk SiC [13] and on the other hand, the recent-theoretical-prediction of 100-times reduction of the thermal conductivity at the nanoscale, due to the increased role of phonon scattering, will lead to an even more increased thermoelectric figure of merit ZT [14].

In the present paper, a comprehensive review of the current status of SiC NW technology is given. In the first section, a description of the different growth methods is presented. Four different principles for the SiC NW growth have been used up to now: the conversion of C- or Si-containing 1D structures to SiC ones, the vapor-liquid-solid (VLS), the vapor-solid (VS) and the solid-liquid-solid (SLS) mechanisms. The second section is dedicated to the results of the SiC NW physical characterization. The third section deals with the device and applications related effort. The SiC-NWFETs are the main focus of the device relative research reflecting the importance given in nanoelectronic applications in the NW-related area. An important effort is also dedicated to the use of SiC NWs as field-emission cathodes. The last section deals with the main conclusions from the up to now SiC NW related research and the prospects of this field.

2. SiC NW material growth

It is well known that bulk SiC crystallizes under many different forms called polytypes. The most common are the cubic form (3C or β), the two hexagonal ones (4H and 6H) and some rhombohedral forms (9R, 15R and 21R). The cubic polytype is the most stable at low growth temperatures [15] despite the fact that the 6H- polytype is the most stable from thermodynamic equilibrium point of view. For this reason, 3C-SiC NWs have been formed in the vast majority of bibliographic studies and in the remaining text the mention of SiC would correspond to the cubic polytype otherwise the polytype will be explicitly mentioned.

Many of the produced SiC-based NW structures are covered by an oxide layer and some by C-rich phases i.e. they consist of a continuous crystalline nanowire encapsulated in a sheath of a different crystalline material and they are rather one dimensional (1D) coaxial nanocables than nanowires. However, for many of them the sheath is a thin native oxide with minor influence on the physical properties and often removed during device fabrication. In the following, all grown structures will be mentioned as nanowires for the shake of simplicity.

In the beginning of 90's, 3C-SiC nanowires were produced by several routes: carbothermal reduction of silica, decomposition of organic silicon compounds, and reaction between silicon halides and CCl_4 [16, 17]. Generally, these nanowires had diameters of about half a micrometer (not suitable for micro/nanoelectronic applications) and they will be not considered in the following.

2.1. Conversion of C-containing or Si 1D structures to 3C-SiC ones.

2.1.1. Conversion of carbon nanotubes (CNTs) and C-fibers. A series of experiments of SiC NW formation has been made using the reaction of carbon nanotubes (CNTs) with Si-rich vapors like that produced by the evaporation of solid SiO or SiI_2. Zhou and Seraphin [18] were the firsts to develop such a process but the size of the SiC NWs were typically one order of magnitude larger and longer than that of the CNTs. H. Dai et al. [19] succeeded to synthesize SiC NWs whose diameters were similar to the diameters of the CNTs (2-30nm). The spatial orientation of the SiC NWs was randomly distributed in agreement with that of the initial CNTs. Pan et al. [7], using the same growth approach but spatially oriented CNTs as starting material, have demonstrated the synthesis of oriented SiC NWs, which could subsequently be evaluated for field emission applications. A systematic time-dependent TEM analysis revealed the key growth steps of the CNTs conversion to SiC [20]. The reaction is not a substitution chemical reaction and the CNT structure (cylinders or bamboo) has a strong effect on the reactions. The segmented bamboo-like structure causes the reaction to start on the nanotube external surface towards the interior and progressively transform the CNTs into a SiC-based NW while no reaction takes place inside the nanotubes. In the case of cylindrical nanotubes, different substitution reactions could take place both inside nanotubes and on external surfaces [20] as the Si can diffuse through the open ends of the tubes or through defects from the walls to the interior.

Conversion of C-fibers has been also applied for SiC NW fabrication [21, 22]. C-fibers have been produced by electrospinning of polyacrylonitrile (PAN) nanofibers at ambient temperature and subsequent carbonization at 700ºC in [21]. The nano- fibers were further heated for 1 h at 1600ºC in

an atmosphere of SiO vapor and Ar. According to the same authors, the advantage of C-fiber conversion process is that single-crystalline nanowires can be obtained in a relatively large quantity and that these NWs have a uniform cross-section, well-ordered structure and a very low concentration of stacking faults. The SiC NWs produced by this C-fiber conversion (as well as by the CNT conversion) contain no catalyst in comparison with SiC whiskers or nanowires synthesized by the VLS mechanism.

2.1.2. Conversion of Si 1D structures.

It is very well known that 3C-SiC is formed on Si substrates by conversion of a heated Si surface in the presence of C-containing species although the resulting layer is highly defective due to the large lattice constant and thermal coefficient mismatch between the two materials [23, 24]. However, in the case of SiC NWs these problems are expected to be of reduced importance, as the induced strain can be coherently accommodated through lateral relaxation. The first formation of SiC NWs by Si NW conversion with a carbon-containing precursor has been reported as a side effect during the deposition of CNTs on Si NWs [25]. A more systematic work to synthesize SiC nanowires by conversion of VLS-grown Si nanowires has been reported by Tsakalakos et al [26]. The grown SiC NWs were polycrystalline although of better quality than that of the previous first study [25]. Tsakalakos et al, by performing thermochemical calculations, also showed that the Si nanowire conversion to SiC is kinetically limited below ~1100 °C despite the fact that the corresponding Si layers conversion is thermodynamically favorable over a wide temperature range. Similar results in terms of SiC NW material quality have been obtained in a recent study following the same approach [27], showing that the optimization of this process would require an important effort.

2.2. 3C-SiC NW growth based on vapor–liquid–solid (VLS) mechanism

The VLS growth process is the most well-established method to produce nanowires. The VLS mechanism is introducing a catalytic liquid alloy phase which can rapidly adsorb a vapor to supersaturation levels and from which, crystal growth can subsequently occur from nucleated seeds at the liquid-solid interface. Nanoclusters are used to define nucleation (nucleation seeds) and subsequent nanowire growth. The use of catalyst allows the formation of the liquid phase at low temperatures and a fast growth contrarily to the very slow growth of a crystal through direct adsorption of a gas phase on to a solid surface. The NWs grown by VLS are characterized by the systematic presence of catalyst particles on their tips.

Various growth configurations using the VLS mechanism have been employed for the SiC NW growth. Gas as well as solid Si and C-containing sources have been used while in most cases, metal catalysts have been available on the substrate surface where NWs are deposited or in mixture with the Si and C- fluxes.

The first experiments of small-diameter SiC NWs growth, based on VLS mechanism, were implemented through Hot Filament Chemical Vapor Deposition (HFCVD) in a reacting, by the presence of atomic hydrogen, ambient. This was contrary to the inert atmosphere commonly used for the growth of CNTs or Si NWs by various methods. In [28], SiC NWs were produced by the VLS mechanism in a HFCVD system using solid sources of Si and C. The process was catalyzed by metallic particles from impurities in the solid source (solid plate). The atomic hydrogen etched the solid plate and produced gaseous hydrocarbon radicals (CH_x), hydrosilicon radicals (SiH_x), or organosilicon molecules. When these vapor molecules reached the vapor–liquid surface, they were dissociated into Si and C atoms. These atoms were dissolved into the liquid catalyst, which upon supersaturation, induced solid SiC precipitation onto the Si substrate. As precipitation continued, the NW grew, lifting the catalyst particle from the substrate and forming a NW. The NWs were 10–30 nm in diameter and less than 1 μm in length and they consisted of a crystalline 3C-SiC core with an amorphous silicon oxide shell layer and grew along the [100] direction according to the High Resolution Transmission Electron Microscopy (HRTEM) measurements. Indeed, the HRTEM images have shown that, in the NWs core, the lattice fringes with 0.25 nm of (111) plane spacing were in 45º

with the NWs axis and the authors concluded that the NWs are [100] oriented. It is one of the very few cases where an [100] orientation of the SiC NWs is reported.

The relatively low value of NWs diameter could explain this discrepancy. The large diameter NWs are [111] oriented and the smaller diameter [100], like in the Si case [29]. Indeed, nanowires generally grow in the crystal direction that minimizes the total free energy, which in most cases, is dominated by the surface free energy of the interface between the semiconductor and the metal catalyst. For diamond and zinc-blende crystals it has been widely observed that the semiconductor–catalyst interface often forms a single surface at the lowest-energy (111) plane and thus, nanowires tend to grow in the [111] direction for most growth conditions [30]. Other low-index growth directions have been occasionally reported including [001], [110] and [112] depending mainly on the diameter of the NW. An excellent review on the control of NW orientation is given in [29].

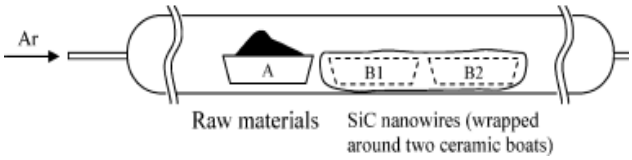

Figure 1. Schematic image of the preparation apparatus for solid source VLS process. The slurry solution was placed in a common ceramic boat (denoted as A), which was then pushed into the center of a tubular corundum furnace, with another two empty ceramic boats (denoted as B1 and B2) placed downstream of boat A. (Reproduced with permission from [32]. © American Chemical Society)

A typical VLS-based NW growth configuration at 950ºC in an horizontal hot-wall CVD furnace has been applied by Seong et al. [6, 31] to fabricate SiC NWs with ~100 nm of diameter and several μm of length for subsequent NWFET fabrication. Thermally oxidized Si wafers with a 2 nm layer of Ni, deposited by sputtering, were used as initial substrates. Methyltrichlorosilane (MTS, CH_3SiCl_3) was chosen as a source precursor due to the 1:1 ratio of Si and C and the low decomposition temperature and H_2 was used as the carrier gas.

VLS was also the mechanism for the preparation of large areas of centimeters-long SiC nanowires by pyrolysis of a polymer precursor with ferrocene catalyst (slurry solution formed by introducing liquid polysilacarbosilane and some ferrocene into activated carbon powder) [32]. The furnace (figure 1) was heated to 1300ºC at 10 ºC /min in a flowing ultra-high-purity Ar atmosphere at a very low rate, maintained under these conditions for 3 h, and then allowed to cool to room temperature naturally.

2.3. 3C-SiC NW growth based on vapor-solid (VS) mechanism

The VS mechanism of SiC NW growth, correspond to the case where Si- and C-containing gaseous precursors react on a surface (or its near proximity) of a solid to form SiC NW. It is similar as mechanism to the vapor-phase-growth mechanism of thin films or even to the aforementioned 2.1 category of Si or C-containing 1D structures conversion, with the difference that growth starts at nanometric nuclei created in-situ and it proceeds according one crystallographic direction. This crystallographic direction is either characteristic of the crystal anisotropy or thermodynamically favorable. The nanometric nuclei are induced by the supply/formation of Si- and/or C-containing nanoparticles on the surface of the solid. Thus, an appropriate and well-controlled growth configuration has to be employed in order to form nanosize nuclei for subsequent NW growth on top of them as well as to ensure growth along one axis. Various gas precursors and experimental configurations have been used without any presence of a metallic catalyst. The latter could be an advantage to the other methods using a metal catalyst since the presence of the catalyst in the final NW is considered as deleterious for device application. The oxygen presence in the precursors seems necessary for the reaction in most reported studies. This is similar with the Si NW case where Si NW growth could be achieved without the usage of metallic catalyst, when SiO_2 instead of pure Si was used [33] as Si source. Nevertheless, SiC nanoribbons were synthesized by a reaction of silicon vapor and carbon black powder at 1500ºC in Ar atmosphere at atmospheric pressure [34] i.e. without any

obvious presence of oxygen although the temperature of reaction was higher than that in VLS experiments and the presence of oxygen in small quantities cannot be excluded.

The above oxide-assisted growth has been also applied by Bechelany et al [35] in the case of SiC NW growth. They have proposed a VS-based method without usage of catalyst for the mass production of 3C-SiC-based nanostructures, which is capable for the fabrication of large amounts of 3C-SiC NWs with tuneable geometric features and surfaces and that could potentially be chemically modified in situ. The experimental set-up (Figure 2) consisted of an alumina boat containing polypropelane (PP), followed by a second alumina boat containing an equimolar mixture of Si(s) and SiO_2(s), which was partially covered by a graphite condensation plate. The entire setup was placed into the hot-zone of the alumina tube of a convective furnace. All of the experiments were conducted under argon low flow rates at temperatures as high as 1400°C, and the NW growth last several hours. Following this method and by adjusting the concentration of the precursors, radial heterostructures such as SiC/SiO_2, SiC/BN and SiC/C could be prepared. Note that the use of solid precursors decrease substantially the fabrication cost of SiC-based 1D structures compared to conventional CVD products obtained by using high-purity gaseous reactants.

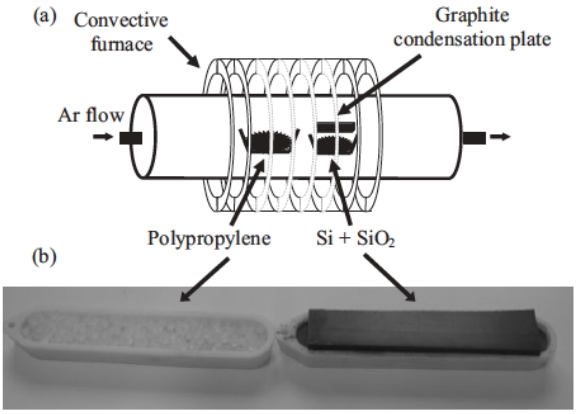

Figure 2. a) Experimental setup designed for the growth of SiC@SiO_2 nanocables; b) picture of the two alumina boats with the graphite condensation plate. (Reproduced with permission from [35]. © 2007 Wiley-VCH)

In another report [36], an analytical study of the possible reactions between intermediate gas phases, the reaction steps, and the surface energy minimization has been presented.

2.3.1. VS in reducing environment. In general a reducing environment enhances the catalyst free growth and can result in SiC-NW-formation-temperatures lower than 400ºC as it was shown in [37] and [38]. However, a subsequent cleaning, either in hot (180ºC) chemical environments or by heating (600ºC) on air, has been necessary to separate the SiC NWs from other by-products of the reaction. The critical point of these low temperature chemical growth methods is the usage of an autoclave, which confines the reaction vapors. In both studies, $SiCl_4$ and CCl_4 have been used as silicon and carbon precursors and Na as a co-reductant element. In [37], the addition of sulphur led to further decrease of the required temperature down to 130ºC due to the catalytic role of the Na_2S formed during the reactions.

2.4. 3C-SiC NW growth based on SLS mechanism

In the solid-liquid-solid mechanism, called root growth, a metal-rich catalyst remains on the surface of the silicon substrates during the entire process and the substrate itself serves as a silicon source without any additional Si source from outside. The carbon is provided either by depositing on the Si substrate a metal catalyst-C thin layer like Ni-C [39] and Fe-C [40] or by carbothermal reduction of WO_3 proving a reducing environment [41]. Then by heating at temperatures higher than 1000ºC, SiC nanocables are formed in most cases with SiC NW as core and with SiO_x and a-C as sheath material.

On the contrary to the VLS mechanism, different orientation and polytype phase NWs are grown with the SLS. Indeed, except the usual [111] orientation [41], ([100] orientation [40] and even hexagonal phase [39] NWs have been reported as products of the SLS mechanism.

In addition, SLS seems a convenient method for fabricating SiC nanocables with a good control on the sheath material. Note that the bandgap and thickness of the latter [41] as well as the density of the nanocables/nanorods/NWs [40] affect directly field emission properties.

2.5. 6H-SiC NW formation.

Li *et al* first reported the synthesis of cone-shaped, 6H–SiC, [$10\bar{1}0$]-oriented, nanorods by an arc-discharge process [42] between a SiC rod (anode) and a graphite plate (cathode). The 6H-SiC NWS were formed on the surface of a Si wafer held, by a Ni-Al alloy bar-like holder, on top of the SiC anode. The diameters of the NWs thin ends are about 10–30 nm, while their thick ends range from tens of nanometers to more than 100 nm, depending on their lengths (maximum 1 μm). In a subsequent study, Gao *et al* [43] reported the synthesis of Al-doped 6H–SiC, [$10\bar{1}2$]-oriented, nanowires 150–300 nm in diameter by catalyst-assisted ($FeCl_2$) pyrolysis of polymeric precursors. Wei et al [44] succeeded also to obtain 6H–SiC, [$10\bar{1}0$]-oriented, NWs but with a lower diameter of 5–200 nm and a length of tens to hundreds of micrometers by using microwave heating of a xerogel containing Si and C precursors as well as nano-Al powders.

For the formation of 6H–SiC nanowires, the VLS [42, 44] and the SLS [43] mechanisms have been proposed. However, only in one case [42], Fe alloy particles have been found on the tips of the NWs probably due to the fact that a purification process has been performed in the two other studies after the NW growth and prior to physical characterization. Moreover, the 6H-SiC NWs were Al-doped in all cases and according to Wei et al [44] 6H-SiC NWs could not be obtained without the usage of nano-Al powders. The Al content was high enough to result in a decrease of the SiC lattice constant. The existence of high enthalpy Al-containing droplets during the growth process and the incorporation of Al in the growing crystal are assumed responsible for the formation of 6H-SiC than the stable 3C-SiC phase.

3. SiC NW physical characterization

Since the main effort on SiC NWs has been dedicated to material growth there is a plethora of data relative to structural characterization of the grown nanowires and much less on optical and especially on electrical properties. Representative data of each characterization method are given in the following subsections.

3.1. Structural characterization of SiC NWs

3.1.1. Optical and Scanning Electron Microscopy (SEM). The SiC NW surface morphology has been

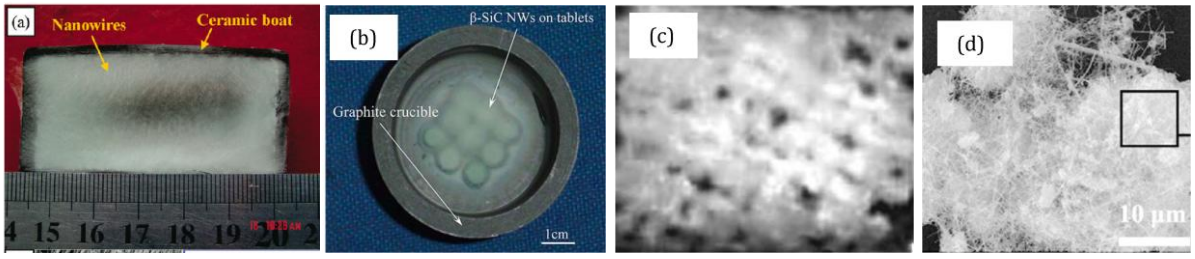

Figure 3. Optical camera (a, b, c) and low magnification SEM (d), photos showing the morphology of the SiC NW containing product. (Photos (a), (b), (c) and (d) reproduced with permission from [32], [45], [46] and [44] respectively).

investigated in all reported studies by SEM and in few cases by optical microscopy. In figure 3, typical macroscopic images of the SiC nanowires growth product are reported [32, 45, 46, 44]. These images correspond to large quantities of produced SiC NWs and the product has a cotton- or foam-like

morphology. In the case of a small quantity of produced NWs on a substrate (typical configuration for VLS-based growth) the substrate has just a hazy appearance.

However, higher magnification images show that there is a large variety of SiC-NW-containing-

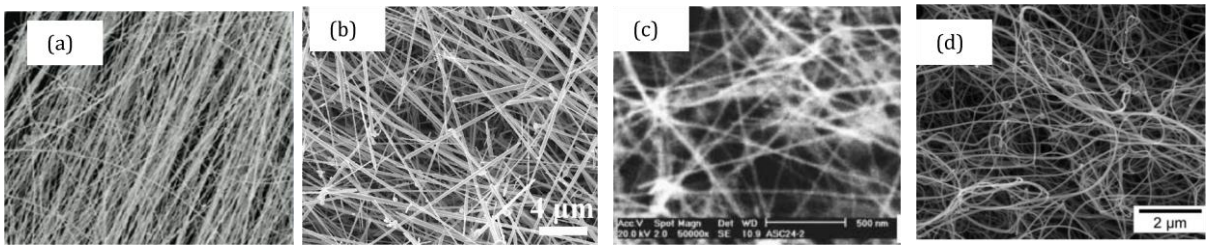

Figure 4. SEM images of different SiC-NW-containing products. (a) "mostly aligned" NWs, (b) "straight interlaced" NWs, (c) "straight interlaced with entanglement points" and (d) "curved/buckled and interweaved" NWs. (Photos (a), (b), (c) and (d) reproduced with permission from [32], [43], [46] and [35] respectively).

product morphology and the hereby-reported surface morphology categories represent the large majority of the studies. Figure 4 shows typical SEM photos from the different categories of NW shapes. NWs are either straight mostly aligned towards one direction (figure 4a, [32]) or straight and interlaced between them (figure 4b, [43]) or straight and interlaced but with entanglement points (figure 4c, [46]) or curved/buckled interweaved between them (figure 4d, [35]). There is not an obvious correlation between growth mechanism and these categories.

High resolution SEM (Figure 5; [36], [44], [42]) has been also used for determining the NWs diameter and length as well as for elucidate the growth mechanism by checking whether metals are present on the NWs tips (Figure 5d). The latter has been complemented, in most cases, by Energy Dispersive X-Ray Spectroscopy (EDS) measurements allowing the detection of the elements present in the NWs. In [36], the morphology of the SiC nanowires has been tuned to cylinder, hexagonal prism

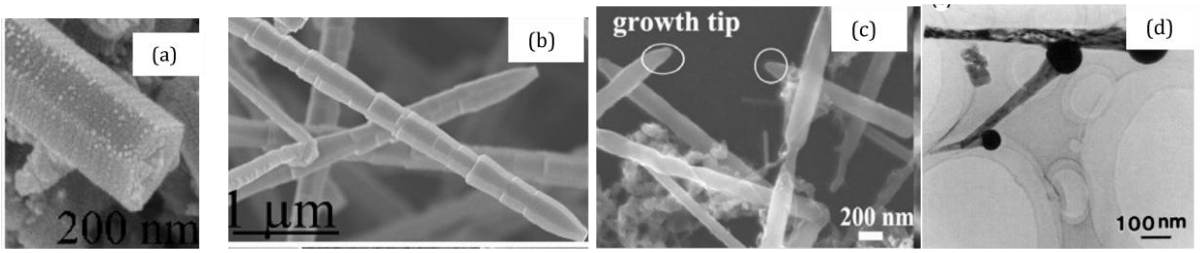

Figure 5. SEM images of different shape individual SiC NWs. (a) hexagonal prism NWs, (b) bamboo-like NWs, (c) conical growth tips of cylindrical NWs and, (d) increasing diameter nanorods with spherical metal catalyst nanoparticles on their tips. (Photos (a)-(b), (c) and (d) reproduced with permission from [36], [44] and [42] respectively).

(Figure 5a), or bamboo shape (Figure 5b) by simply altering the reaction temperature from 1470ºC, 1550ºC to 1630ºC, respectively. The results have been explained in terms of equilibrium shapes at each temperature.

3.1.2. X-rays Diffraction (XRD). Almost all growth studies of SiC NWs make reference to XRD *θ-2θ* characterization results. A typical XRD spectrum ascribed to β-SiC nanowires is shown in figure 6 [41]. The peak at 35.7º corresponding to the [111] orientation is preponderant and many authors have concluded that this is the main orientation of the grown nanowires. Peaks attributed to the Si substrate and the stacking faults (sf) of SiC were also found in some cases as in Figure 6 although they are not present in the spectra reported in most studies. Additional peaks corresponding to other

crystallographic planes - usually at 41.5º((200) planes), 60.1º((220) planes) and 71.8º((311) planes) - have been observed in all experimental studies.

Figure 7 shows the XRD pattern measured from 6H-SiC NWs [44]. The observed peaks have been indexed as those of hexagonal structure crystal (6H–SiC). The authors have compared the spectrum

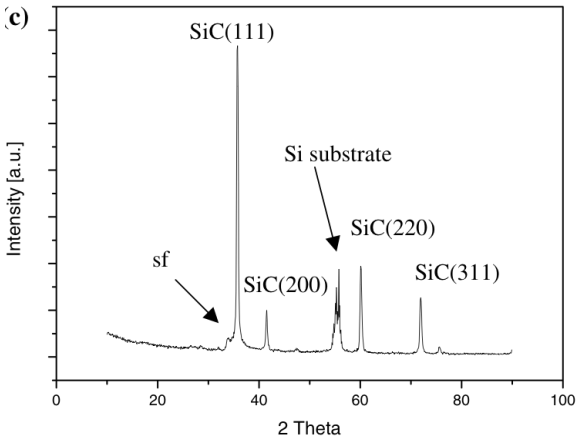

Figure 6. XRD pattern obtained from 3C-SiC nanowires. The crystal orientations [111], [200)], [220] and [311] were observed; sf indicates stacking faults in the SiC crystal. (Reproduced with permission from [41]. © 2010 IOP)

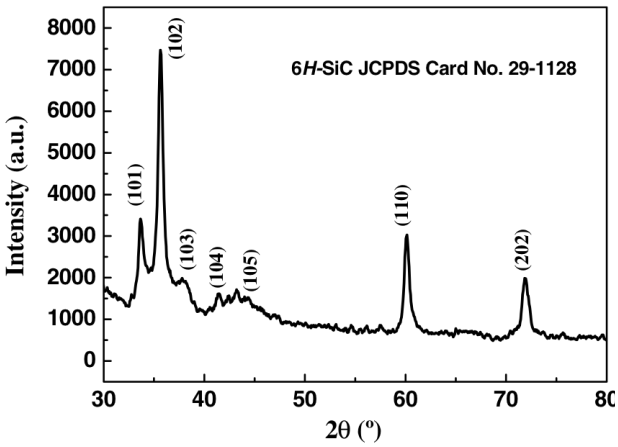

Figure 7. XRD pattern obtained from 6H-SiC nanowires where all the peaks can be indexed as that of 6H-SiC. (Reproduced with permission from [44]. © 2010 IOP)

with the corresponding one of bulk 6H-SiC and they have concluded that, the lattice parameters of the nanowires decrease without mentioning any quantitative result. The same conclusion has been obtained in [43], although the change in angle was of the order of 0.1º. This is attributed to a large incorporation of the big Al ions in substitutional sites of SiC resulting in a strained crystal and in a lattice constant change. Moreover, according to the authors, the broadening of the diffraction peaks is attributed to the small diameter of nanowires and to the overlapping of the diffraction peaks. However, the existence of aluminum atoms at interstitial sites could also contribute to this broadening [47].

A series of remarks can be drawn on the reported XRD spectra in the different experimental studies.

The first one, is that the spectra contain peaks corresponding to diffraction at different planes. In the case of well aligned nanowires like that of Figure 4a, the multiple XRD peaks could be an indication of a textured morphology of the nanowires themselves or the existence of single crystalline nanowires with different orientation. In all other cases, the measured spectrum is rather similar to that obtained in a powder measurement configuration in which the (111) peak or the $(10\bar{1}2)$ peak is the preponderant one for the 3C-SiC and 6H-SiC cases respectively. Both peaks appear at almost the same angle.

Indexing the XRD spectra and defining the polytype of the grown NWs is not straightforward in many cases. Indeed, by comparing the standard powder XRD spectra (JCPDS cards) between the 3C- and the 6H- polytypes, the main difference is the appearance, in the case of the 6H-SiC, of the $[10\bar{1}1]$ peak at 34.2º. A series of other peaks (38.2º-$(10\bar{1}3)$ planes, 41.5º-$(10\bar{1}4)$ planes, 65.8º-$(10\bar{1}9)$ planes and 73.6º-$(20\bar{2}3)$ planes) are present in the spectra from the 6H-SiC only but they are hardly distinguishable. However, there are cases where the peak at 34.2º has been also observed in the case of cubic SiC NWs (see figure 6) due to the high number of SFs (equivalent to hexagonal inclusions) and in this case, the conclusions on the polytype of the NWs have to be corroborated with corresponding TEM results.

The sharpness of the diffractions peaks especially for small diameter NWs can't be used as a quality indicator since a broadening can be induced in this case by a size effect or surface states or even by an overlapping of peaks.

3.1.3. Transmission Electron Microscopy (TEM). Most of the SiC NW experimental studies report TEM observations. The TEM electron diffraction can distinguish between a textured morphology of the nanowires themselves or the existence of single crystalline nanowires with different orientation since polycrystalline rings or a spotty pattern characteristic of the orientation of the nanowire under examination, would be observed in the first and the second case respectively. Nevertheless, a large number of measurements in different locations of the same nanowire as well as on different nanowires have to be examined by TEM in order to have enough statistical data for drawing a conclusion on this point.

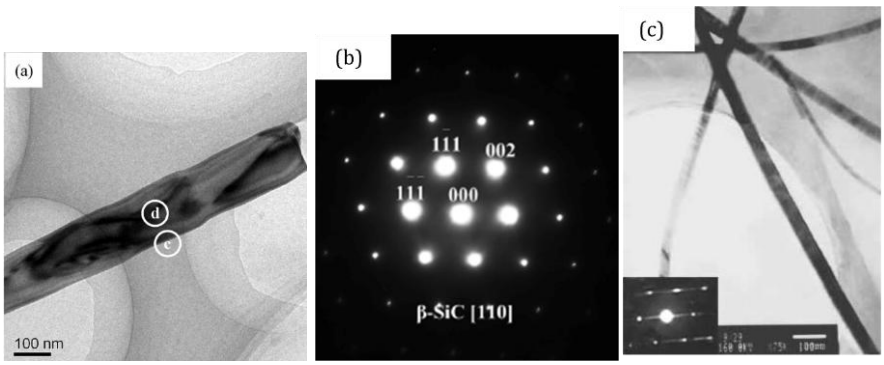

Figure 8. TEM image (a) and the corresponding indexed SAED pattern (b) of a single crystalline β-SiC NW; (Reproduced with permission [32]. © American chemical society). The nanowires are without any coating of amorphous material. The insert is the selected-area electron diffraction (SAED)of the nanowire exhibiting streaks of stacking fault structures; (Reproduced with permission from [46]. © Springer)

Figure 8a shows the TEM image of a rather good quality nanowire and the corresponding indexed selected-area electron diffraction (SAED) pattern (figure 8) with clear diffraction spots indicates that the NWs are single crystalline and that grew along the [111] direction [32]. However, the SiC NWs contain a large number of stacking faults (SFs) and in some cases

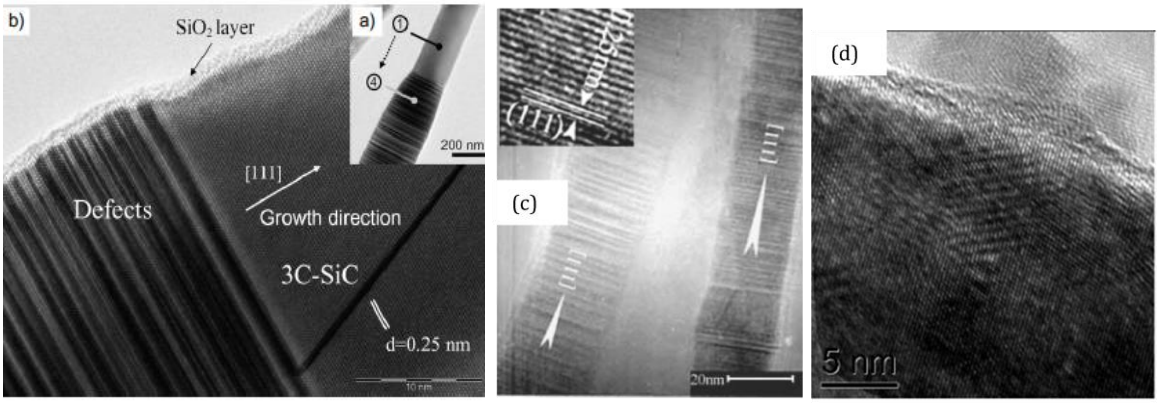

Figure 9. TEM and HRTEM observations from defected SiC NWs. a) TEM image of a typical SiC NW exhibiting an SF area (dark part) and a pure 3C-SiC section (bright part). b) High-resolution image of the interface between those two crystallographic zones. c) HREM image of two nanowires lying along the [111] direction with the sequence of SFs occupying their whole volume. d) SiC NW area with various orientation defects. (Photos (a) and (b) reproduced with permission from [35] © 2007 Wiley-VCH; (c) reproduced with permission from [46]. © Springer; photo (d) reproduced with permission from [32]. © American Chemical Society)

their density is enough to result in a streaked diffraction spots as in the case of figure 8c [46]. Planar defects (mainly stacking faults and twins) are common in bulk SiC due to the polymorphism of this material and they can be viewed as nanoscale polytype inclusions within the pure 3C-SiC phase. Note that the 3C-SiC has a negative SF energy - the only material with ZnS presenting negative SF energy - and it is very easy to generate SFs in 3C-SiC even under the thermal stress created by the electron beam in the TEM [48].

Figures 9a to 9d show HRTEM images of SiC nanowires with crystal defects mainly SFs. The spatial extension of the defected zone can be small as in the case of figure 9d [32] or NW-diameter-large (figure 9a and b) [49] or even extending in the whole NW (figure 9c) [46]. In most cases the SFs are perpendicular to the nanowire axis (Figure 9a, b and c). The diameter of the NW-diameter-large-SFs-zones is larger than that of the defect-free zones giving a faceted shape in the NW surface with each facet belonging to a SF section. In the extreme case the defected zones are looking like periodic along the NW axis giving a bamboo-like shape to the SiC NWs [50]. The large diameter of the defected zones is quite probably due to the strain relaxation in these areas [46, 36] as the stacking faults are generally thought to originate from thermal stress during the growth process.

HRTEM images show typically the lattice fringes with 0.25 nm of (111) plane spacing of the 3C-SiC crystal (Fig 9). Moreover, in most cases, an amorphous sheath of about 2-5 nm is usually formed on the surface of the SiC nanowires as it is shown in Figure 9a. According to the EDS analysis, this is an amorphous SiO_2 layer, which in many experimental studies was rich in C.

Stacking faults and twins (Figure 10) have been also observed in 6H-SiC NWs [44]. Strain is

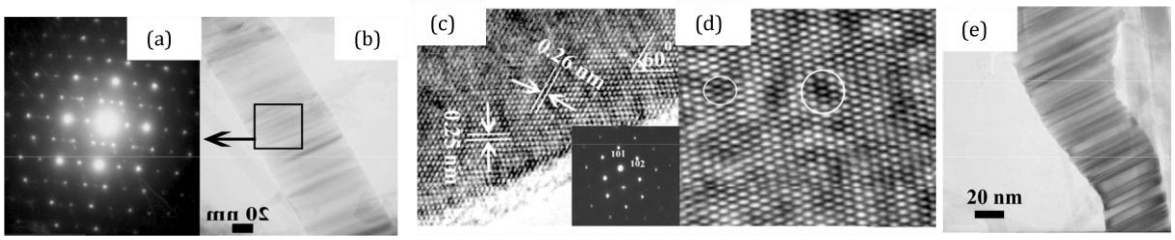

Figure 10. TEM image of a 6H–SiC nanowire (a) and the corresponding SAED pattern (b), showing the nanowire possessed twinning structure. (c) HRTEM image from a NW and the corresponding indexed SAED pattern in the insert. (d) Simulated image of the ordered structure, obtained from a digital diffractogram based on the Fourier transform of previous figure (c). (e) NW with stacking faults. (Reproduced with permission from [44]. © 2010 IOP)

believed to be the principal driving force for the formation of the twins observed in SiC [23] and according to Wei et al [44] the strain arises from the non-equilibrium thermal conditions in the nanowire growth process. However, a high Al incorporation in the crystal, as it is the case, induces strain in the crystal and can be the cause for the high density of twins and SFs (see corresponding discussion in section 3.1.2 above). In figure 10c the lattice fringe spacing are 0.26 and 0.25 nm, in good agreement with $(1\bar{1}0\bar{1})$ and $(10\bar{1}2)$ planes of bulk 6H-SiC, where a=0.308 nm and c=1.509 nm. The image of figure 10d shows a uniform Al doping of the nanowires with bigger lattice fringe spacing around each Al atom (white circles in Figure 10 d) as the Al atom has substituted the Si atom. Figure 10e shows that for many 6H-SiC NWs the whole volume is occupied by stacking fault areas.

3.2. Optical characterization of SiC NWs

Quantum confinements effects (QCE) such as blue shifts in PL spectra and red shifts in Raman spectra [51] are expected in the case of thin enough NWs. Wu et al [52] estimated the Bohr radius to be 2.7 nm, so only such NWs with same order of size would exhibit a strong quantum confinement effect. Even for small enough diameter NWs, surface-defect states do not allow the observation of quantum confinement effects. Thus, it is not expected to observe such effects since, the large majority

of experimental studies deal with large (>20 nm) SiC NWs. Despite these expectations blue shifts in PL spectra and red shifts in Raman spectra have been observed in most studies and the authors of these studies have proposed various explanations.

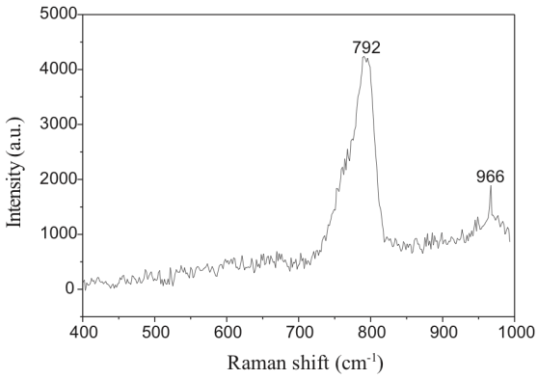

Figure 11. Typical Raman backscattering spectra of cubic β-SiC nanowires recorded at room temperature. (Reproduced with permission [46]. © Springer)

3.2.1. Raman spectroscopy. Raman spectroscopy is one of the best-understood techniques to characterize bulk SiC polytypes. In the case of SiC NWs, many different Raman studies have been reported [32, 46, 49, 53, 54]. A typical example is shown in figure 11 (after [46]). The observed peaks correspond roughly to the transverse optic (TO) and longitudinal optic (LO) vibrational modes of 3C-SiC at the Γ point of the Brillouin zone. However, with respect to bulk reference material (795 cm^{-1} for the TO mode and 972 cm^{-1} for the LO mode), the Raman frequencies in NWs are shifted. As already said, such shifts of the lines and a stronger intensity of the TO(Γ) component in comparison to the LO(Γ) one were sometimes attributed to QCE [46, 53]. However, the diameter is too large (well above 10 nm) and unresolved polytypic admixture could be on the origin of these peaks since stacking faults (equivalent to a polytypic admixture) have been already observed using HRTEM (see Sect. 3.1.3 above). Resolving polytypic admixture with Raman spectroscopy is not so easy. A detailed study of one individual SiC NW is necessary, with spatial resolution better than the average extension of the individual polytypes.

Such a work has been done by Bechelany et al [49]. Moving the Raman spot position on top of a single NW attached to the apex of a tungsten tip coated with a thin gold layer, different spectra can be recorded depending on the spot position. In figure 12, Raman spectra for different probe locations on a single, 1 μm diameter, NW are shown. If the NWs were free of SFs or polytypic admixture, only the TO and LO modes of the main SiC polytype (3C-SiC in this case) should be observed with experimental values characteristic of the Γ point of the Brillouin zone, regardless of the probe position. However, a peak centered at 786 cm^{-1}, which is not present in bulk 3C-SiC, corresponding to the TO modes of various polytypes, for example 6H (mode $2E_2$) and/or 15R (mode 2E) is present with a high intensity for two locations. The existence of defects is also evidenced by the presence of shoulders like the one observed at 772 cm^{-1} and at 946 cm^{-1}. Their presence emphasizes that local defects play an important role in the resulting Raman spectrum. Indeed, the random stacking sequences of atomic

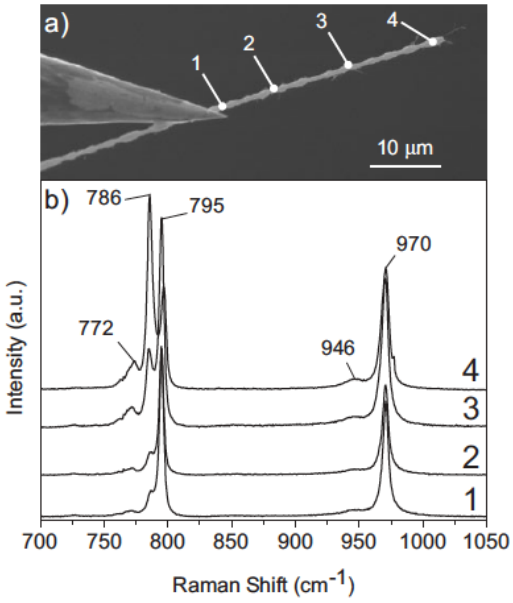

Figure 12. a) SEM image of a 1 μm diameter NW with different probe locations marked by 1, 2, 3, and 4. Locations 3 and 4 correspond to larger diameter zone of the NW with a high density of SFs. b) Raman spectra corresponding to the probe locations noted in (a). (Reproduced with permission from [49] © 2007 Wiley-VCH)

planes like those shown in the HRTEM images of the above figure 9a/b/c, create a virtual local mixture of polytypes, leading to the observation of additional peaks in the Raman spectrum. Moreover, the intensity ratio of this peak at 786 cm^{-1} versus the one at 795 cm^{-1} varies considerably at various locations n the NW. The explanation given for this peak ratio difference was based on the ratio of each crystalline phase or in other words, on the proportion of defects versus the 3C-SiC crystalline phase. It is reasonable to suggest that the signal obtained for the probe in position 1 (see figure 12) comes from a high-quality 3C-SiC area with little contribution from defect areas, while the reverse is true when the probe is in position 4 (figure 12).

According to the same authors [49] some precautions have to be taken during Raman measurements and analysis of SiC NWs. An incident wavelength close to the bandgap energy of the 3C-SiC (2.4 eV), has to be chosen in order to obtain similar intensities for the LO and TO bands in the Raman spectra. The Raman peak position of the LO mode also depends on the crystallographic orientation of the NW versus the incident Raman light and if the SiC NW is fixed perpendicular to the incident light, all of the Raman peaks are shifted by a few wavenumbers to frequencies lower than values found for the corresponding bulk material. Moreover, in order to avoid further frequency shifts resulting from elevated sample temperatures, the power of the laser has been fixed at a low value like10 mW. Only when all the above factors are taken into account, it can be assumed that the observed frequency shifts are only caused by size confinement and/or structural defects.

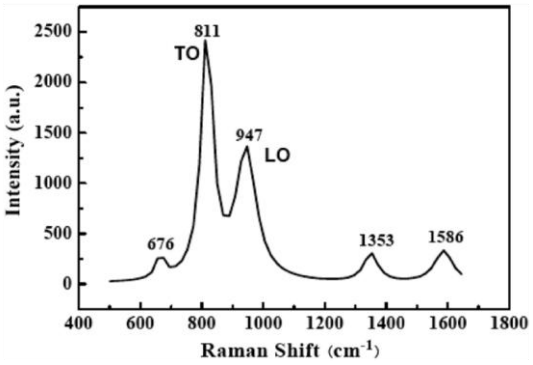

Figure 13. Typical Raman backscattering spectra of hexagonal 6H-SiC nanowires recorded at room temperature. (Reproduced with permission from [44]. © 2010 IOP)

A typical Raman spectrum taken from 6H-SiC nanowires is shown in figure 13 [44]. Five broad peaks at around 676, 811, 947, 1353 and 1586 cm^{-1} are observed in the Raman spectrum. The peak at 676 cm^{-1} has been attributed to defect-induced acoustic (transverse and longitudinal) phonon mode scattering while the broad and asymmetric peaks at 811 and 947 cm^{-1} have been assigned to the transverse optical (TO) and longitudinal optical (LO) modes of the 6H–SiC nanowires, respectively. Note that the bulk 6H–SiC Raman spectrum exhibits three TO phonon modes at 767, 789 and 797 cm^{-1} and two LO modes at 889 and 965 cm^{-1}. Hence, compared with the bulk, the Raman spectrum of the 6H–SiC nanowires had only one TO and one LO phonon mode. The corresponding peaks are very broad extending from 715 to 870 cm^{-1} and from 890 to 980 cm^{-1}. According to the authors, possible origins for this are size confinement effects, stacking faults, Al doping and inner stress from the 6H–SiC nanowire. Two Raman bands at ~1353 cm^{-1} and ~1586 cm^{-1} in figure 13 can be assigned to G and D bands of the graphite layers, respectively.

3.2.2. Fourier Transform Infrared spectroscopy (FTIR). Very few studies of SiC NWs include FTIR measurements. Figure 14 shows he FT-IR transmittance spectrum of the SiC nanowires [32]. The strong peaks at 787.5, 906.1, and 941.3 cm^{-1} correspond to the stretching vibration of the Si-C bonds. The peak at 787.5 cm^{-1} shows a 27.5 cm^{-1} red shift compared with that of the bulk β-SiC, and the

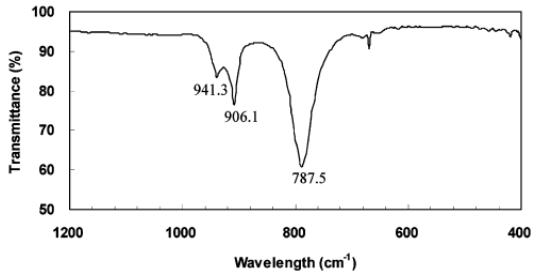

Figure 14. FT-IR transmittance spectrum of the centimeters-long SiC nanowires. The strong peaks at 787.5, 906.1, and 941.3 cm^{-1} correspond to the Si-C bonds' stretching vibration. (Reproduced with permission [32].

authors have ascribed it to size confinement and surface effects [32].

3.2.3. Photoluminescence. Room temperature photoluminescence (RTPL) observations have been reported in a number of experimental works dealing mainly with the growth of SiC NWs and figure 15 shows various RTPL spectra recorded from SiC NWs [6, 53, 55].

In most cases a broad band peak between 430 and 460 nm is present showing a blue-shift in comparison to the RTPL of bulk and/or thin film 3C-SiC exhibiting a near band-edge peak at 540 nm associated with nitrogen doping [56]. This shift is usually attributed to either quantum confinement effects or simple defects that have not been addressed yet [6]. Since the diameter of NWs is much larger than the calculated value of 4.4 nm for the appearance of quantum confinement effects, rather a defect-related mechanism should be responsible for this blue shift. However, the type of these defects

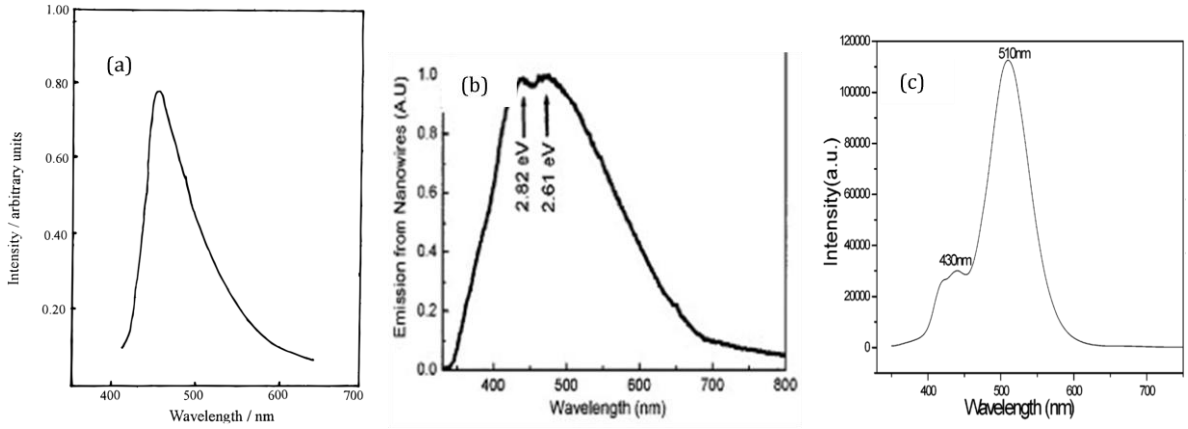

Figure 15. Representative SiC NW RTPL spectra. Left: single peak broad and asymmetric band(Reproduced with permission [55] ©American Chemical Society); Middle: double peak broad and asymmetric band(Reproduced with permission [6] ©American Institute of Physics); Right: clear peak at 510 nm in addition to the blue luminescence (Reproduced with permission [53] © American Institute of Physics).

has not been determined unambiguously up to now. Note that a second peak can contribute to this broad band (see figure 15b) and it is often ascribed [6] to the forbidden transition from the triplet state to the singlet state at the neutral oxygen vacancy (≡Si-Si≡) caused from an amorphous SiO_2 layer usually formed around the NWs. An interesting feature of the blue broad band is its peak wavelength dependence on the NW shape [36] as shown in figure 16. However, these NWs contained large numbers of nanotwins the size of which, change with the shape of the NWs. In this way, the quantum confinement effects result in different peak wavelength for the different shape nanowires.

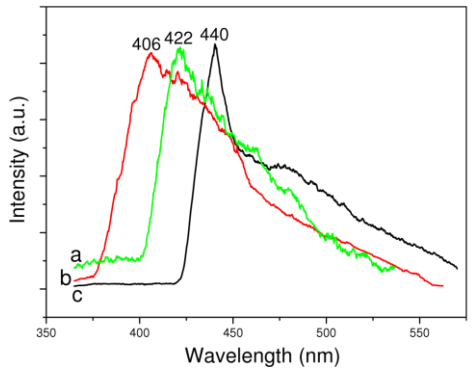

Figure 16. PL spectra of the as-synthesized different morphologies of 3C-SiC nanowires: (a) nanocylinders (b) nanoprisms, and (c) nanobamboos, respectively. (Reproduced with permission [36]. © American Institute of Physics

Another peak observed in PL spectra from SiC NWs is at 510 nm (figure 15 right), which is ascribed to the OH group adsorbed on surface or some localized states [53, 57].

A UV emission around 380 nm has been also observed [54, 58]. Zhang et al [58] performed a detailed study combining PL, Raman and TEM methods to identify the origin of the UV emission at 378 nm and

they attributed it to threefold stacking faults, which structurally resemble to 6H- SiC layers of 1.5 nm thickness embedded in a 3C-SiC matrix. In addition to this UV emission, they have observed the broad emission peak between 450 and 600 nm ascribed to 3C-SiC.

In conclusion, the emission characteristics of the blue broad band and the other emission wavelengths from β-SiC nanostructures, depend strongly on their shapes and sizes as well as on their preparation method inducing various defects and different NW surface states [37].

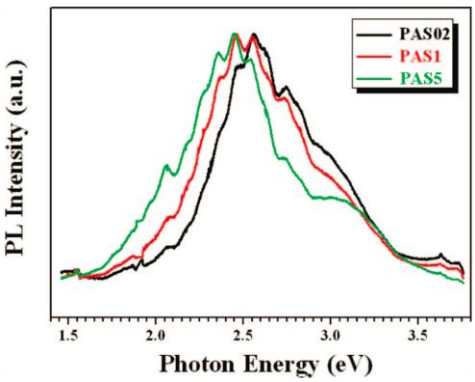

Figure 17. Photoluminescence spectra of 6H-SiC nanowires recorded from different samples with increasing Al concentration (PAS02<PAS1<PA05). (Reproduced with permission [43]. © American Institute of Physics

A high intensity Al-related broad peak ranging from 1.7 to 3.4 eV and centered around 2.5 eV (496 nm) has been observed (figure 17) from 6H-SiC NWs [43]. The peak shows clear red-shifts with increasing Al-doping concentration and it has been attributed to Al-related donor-acceptor recombination in agreement with the PL results of bulk 6H-SiC. Note that pure bulk 6H-SiC crystal exhibits a major emission peak centered at 2.93 eV, ascribed to the band-edge emission while the *n*-type doped 6*H*-SiC shows a major broad PL peak centered at ~2.65 eV, which is usually attributed to a Al-related donor-acceptor recombination process. In another study [44], a broad peak ranging from 2.20 to 3.60eV with the maximum centered at 3.02eV has been de-convoluted to three peaks centered at 2.67 eV, 3.02 eV and 3.52 eV. The first has been attributed to an Al-related donor acceptor recombination, the second to the band edge emission of 6H-SiC and the third to quantum confinement effects in agreement with a similar energy peak observed in the case of 6H-SiC nanoparticles with diameters below 3 nm in the colloidal solutions [59]. Indeed, many NWs, of this study, were not perfect wires, but were actually made up of stacking faults of less than 3 nm width (see corresponding figure 10e). Thus, they act as grains with typical dimensions of only a few nanometers. Consequently, the confinement could take place in three directions and it has been also proposed as explanation for the blue shift of the band edge luminescence (3.02 eV instead of 2.93 eV for the bulk case).

3.3. Mechanical properties and related applications

There are very few studies on mechanical properties of SiC NWs due to the difficulty in their experimental measurement [9, 60, 61, 62].

Wong et al. [9] have performed a delicate measurement of the bending strength and Young's modulus of 20-30 nm diameter SiC nanorods, using atomic force microscopy and lithography techniques. The measured values were 53.4 and 660 GPa, respectively, which are much higher than those of the bulk materials and approach the theoretical values. These increased values of strength have been attributed to a

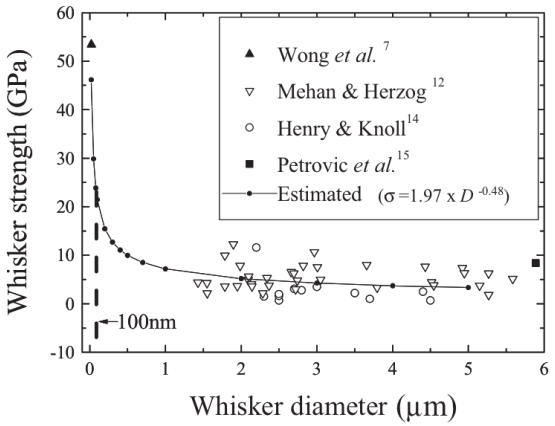

Figure 18. SiC whisker strength as a function of diameter. Note that here is only one experimental point for whisker diameter below 1.5 μm that of Wong et al [9] at 25 nm. The data are fitted with a relationship of the form $\sigma_t = K' D^{-\alpha}$ where σ_t, D are the whisker strength and diameter while K' and α are constants. This relationships is used by the authors of [57] for estimating the strength of their 100 nm SiC NWs. (Reproduced with permission [60] © American Institute of Physics).

reduction in the number of defect per unit length that leads to mechanical failure as compared with larger structures.

In another study [61], an unusually large strain plasticity (i.e. the ability of a material to exhibit an exceptionally large deformation rate during mechanical deformation) of SiC NWs has been observed in situ by a high-resolution transmission electron microscopy technique at temperatures close to room temperature. This unexpected result has been attributed to the reduction of the dimensionality and it has been accompanied by a process of increased dislocation density at an early stage, followed by an obvious lattice distortion, and finally reaches an entire structure amorphization at the most strained region of the NW.

The mechanical resonances of 18-140nm diameter SiC nanowires, which were glued to the ends of tungsten support tips, were electrostatically excited and detected visually in the SEM configuration and then by FE microscopy image processing by Perisanu et al [62 and references therein). The resonator quality factor Q and the Young modulus were determined with a good agreement by both methods although a large scatter in the measured values has been observed from the different nanowires. More precisely, the Q factor varied from 3500 to 160000 and the Young modulus from 230 to 750 GPa.

The high strength values of SiC NWs, indicate their suitability as reinforcing material in composite structures. Yang et al [60] have reported, for the first time, the reinforcement efficiency of 100 nm diameter SiC NWs in ceramic-matrix composites. The average fracture toughness and ultimate flexural strength of SiC-NW-containing composites were respectively 18 $MPa \cdot m^{1/2}$ and 700 MPa, versus 10 $MPa \cdot m^{1/2}$ and 380 for the non-SiC-NW-containing similarly fabricated composites.

Despite these highly interesting initial results, there is a lack of enough experimental studies to have a complete idea of the mechanical properties of SiC NWs. For example there is neither enough experimental data for the size-strength relationship (Figure 18, [60]) nor enough knowledge of the necessary conditions for the appearance of the large strain plasticity.

3.4. Hydrophobic properties and related applications

Super-hydrophobic materials show wide applications in fields of various coatings, textiles, microfluidic systems, self-cleaning of outside wall of a skyscraper etc. The wettability of a solid surface is controlled by surface energy and modifying surface roughness and chemical composition can control the latter. High surface-to-volume ratio structures like NWs are widely investigated for hydrophobic applications since they present a high-energy barrier to form a solid-liquid interface.

The wettability of aligned SiC NW crossed nets has been investigated with a water contact angle instrument by Niu et al [8]. The as-grown SiC NWs were almost hydrophilic with a very low contact angle (147 (±2°) (figure 19b) due to the existing polar OH groups. The chemical composition of the SiC NWs has been modified by employing fluorine-contained perfluoroalkysilane to decrease the surface free energy to values lower than that of water. In this way, the a-SiCNWs exhibited hydrophobicity with a contact angle greater than 156(±2°) (figure 19a). A very weak contact angle hysteresis of less than 5° was observed even after exposing in air for 1 week (figure 19c). Note that a chemically functionalized pure silicon wafer

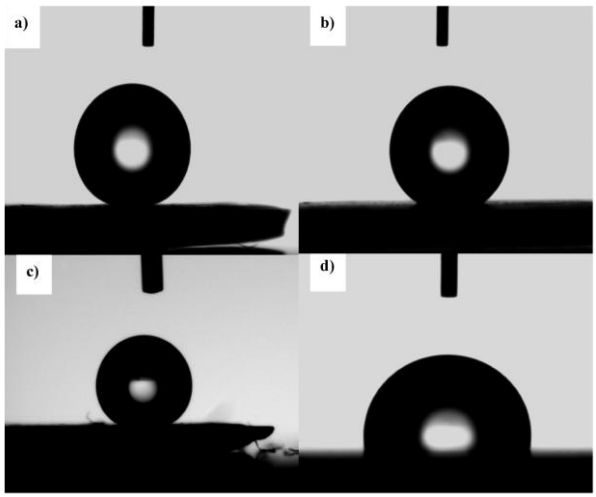

Figure 19. Water contact angles of: (a) chemically modified SiCNWs, (b) as-grown SiCNWs, (c) the sample of (a) after exploring in air for 1 week, and (d) a pure silicon wafer. (Reproduced with permission [8] ©American Chemical Society).

exhibits a low contact angle of 101(±2°) (figure 19d). A tentative sample was scraped off and covered a silicon wafer. The modified new surface displayed a contact angle higher than 140°, which means an increase of nearly 40° compared with a pure silicon wafer and this can be one potential application of SiC NWs. Indeed, coating a silicon wafer with hydrophobic nanowires can result in useful applications in many water-repelling semiconductor devices such as solar cells, radars surface, etc [8].

3.5. Electric and Thermoelectric properties

Understanding the thermal transport in the nanoscale and eventually designing nanostructure-based materials with very high or very low thermal conductivities would have an impact on electronic devices and will also help the design of thermal barriers or new thermoelectric materials. For instance, heat dissipation is important issue for highly integrated devices and nanodevices are suitable for high integration applications. Moreover, bulk 3C-SiC presents high room temperature thermal conductivity in the order of 330 $W \cdot m^{-1} \cdot K^{-1}$ [63] while epitaxial layers on silicon substrate present a lower value around 180 $W \cdot m^{-1} \cdot K^{-1}$ due either to the high density volume and interface with Si defects and/or to the higher surface to volume ratio [64].

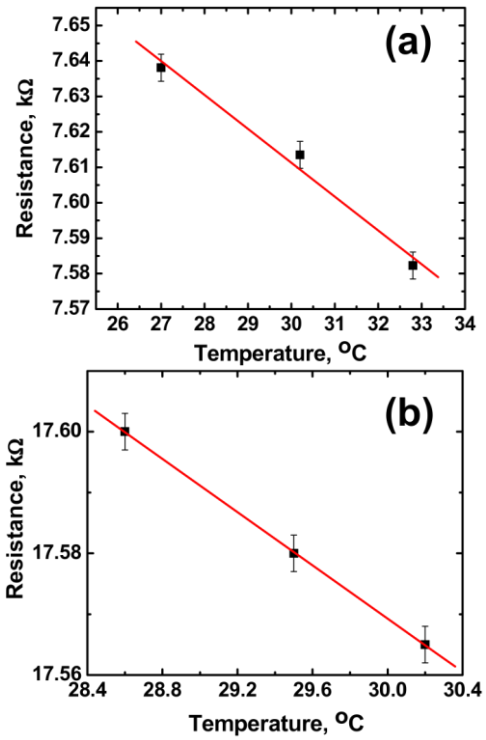

Figure 20. Resistance versus temperature measurement for (a) double β-SiC NW, which has $-10 \circ C^{-1}$ and (b) single β-SiC NW, which has $-22 \circ C^{-1}$. (Reproduced with permission [66] ©IOP 2010).

The thermoelectric properties of 3C-SiC NWs have been investigated both by theoretical calculations [14] and experimental studies [65, 66]. Non- equilibrium classical molecular dynamics simulations for the lattice thermal transport of SiC nanowires with cross sections ~4–17 nm^2 and bulk β-SiC have been performed [14]. According to the results, the thermal conductivity of the nanowires is strongly reduced by one order of magnitude compared to the SiC bulk value. This is due to the confinement, which reduces the phonon mean free path as well as to the phonon scattering on the wire surface and it is the general trend reported for different semiconductor nanowires. For the same reason, the surface structure of nanowires and/or the existence of extended defects (nanotwins, SFs, etc.) is of particular importance for the thermoelectric applications since transport properties will depend to a great extent on surface roughness and can be used to change thermoelectric properties.

T-type nanosensor and HRTEM have been applied for the measurement of the thermal conductivity of an individual silicon carbide (SiC) nanowire of 140 nm diameter [65]. The thermal conductivity of the NW was over 100 $W \cdot m^{-1} \cdot K^{-1}$ at room temperature.

An elegant method of placing a single or double SiC NW on pre-patterned electrodes by using a focused ion beam and a nanomanipulator has been developed, to perform four-probe measurements [66] and measure the resistance of the NWs and its temperature coefficient (figure 20). Then, 3-ω signals were correlated with the thermal conductivity of the NWs. The thermal conductivities of the placed single and double β-SiC NWs were estimated at 82 ± 6 $W \cdot m^{-1} \cdot K^{-1}$ and 73 ± 5 $W \cdot m^{-1} \cdot K^{-1}$, respectively.

4. Devices and applications based on SiC NWs

4.1. SiC Nanowire Field Effect Transistors (SiC-NWFETs)

Theoretical studies on the 3C-SiC-based NWFET operation in ballistic and diffusive regimes by using non-equilibrium Green function formalism (NEGF) and drift-diffusion (DD) schemes, respectively, have shown that the SiC NWFETs have similar performance to the Si-based ones in both transport regimes. Thus, the use of SiC as channel material in NWFETs will not degrade the electrical characteristics, while it will offer all advantages from the SiC physical properties [67, 68, 69].

There are only few experimental studies on 3C-SiC nanowire FETs (see a typical schematic in figure 21a), all presenting similar device performance in terms of transconductance and carrier mobility [6, 22, 67]. The analysis of I–V characteristics (figure 21b) in the first one by Seong et al. [6], has shown that the NWs were highly n-type doped with a resistivity of $2.2 \cdot 10^{-2}$ Ω·cm for 0-V gate voltage and an estimated electron mobility of 15 $cm^2/V \cdot s$. The mobility of carriers was estimated from the transconductance, which is determined from the slope of the I_D–V_G characteristic (insert of figure

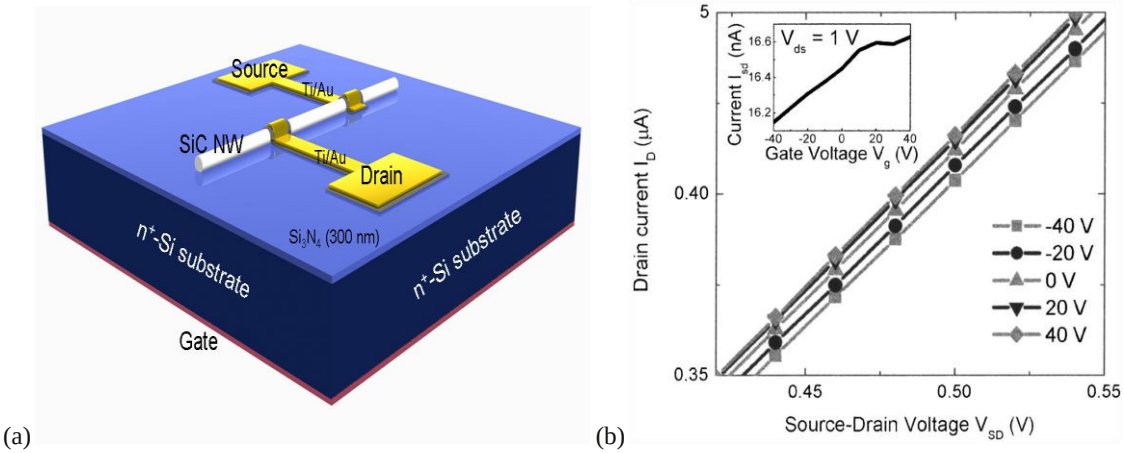

Figure 21. (a) Schematic of a SiC NWFET (Reproduced with permission [66]). (b) I–V characteristics of SiC nanowire FET for different back gating from −40 V to 40 V. In the insert of (b) the I_D–V_G characteristic is presented. (Reproduced with permission [6] © American Institute of Physics).

21b) and the formula $g_m = \frac{dI_{DS}}{dV_{GS}} = \mu\left(\frac{C}{L^2}\right)V_{DS}$, where μ is the carrier mobility, C is the capacitance, and L is the length of the SiC NW. The SiC NW capacitance is given by $C \approx 2\pi\varepsilon\varepsilon_0 \frac{L}{\ln(2h/r)}$ where ε is the dielectric constant, h is the thickness of the silicon oxide layer, and r is the SiC NW radius. The transconductance (g_m) of SiC NWFETs was 1.7×10^{-10} A/V.

Similar results have been obtained later by Zhou et al in an identical study [22] having as only difference the SiC NW growth method (conversion of activated C fibers by using SiO vapors instead of VLS growth in the case of Seong et al [6]). Their SiC NWFET had slightly better performance compared with the results reported in [6] and [67]. The mobility was 15.9 and 6.4 $cm^2/V \cdot s$ when V_{DS} is 0.01 and 0.05 V respectively with corresponding transconductance values 10^{-9} A/V and $5 \cdot 10^{-10}$ A/V.

Nickel was identified to present the lower contact resistance to 3C-SiC NWs [70]. The specific contact resistances for Ni/Au ohmic contacts ($5.9 \cdot 10^{-6} \pm 8.8 \cdot 10^{-6}$ Ω cm^2) were roughly 40 times lower than those for Ti/Au ohmic contacts formed on SiCNWs.

The nanowire/dielectric interface (with high values of fixed charges and interface traps) and the high unintentional doping which leads to a carrier concentration value of the order of 10^{19} cm^{-3} have been presented as possible reasons for the poor device performance (poor gating effect, low carrier

mobility etc) [67]. This doping could originate either from extended defects like the commonly observed in SiC NWs stacking-faults, or from nitrogen contamination during the growth process. The latter explanation is widely accepted while for the former there is a reticence whether the extended defects can dominate the carrier transport. However, in a recent study [71], scanning spreading resistance microscopy (SSRM) technique was used to investigate the electrical activity of the extended defects (antiphase boundaries, twin bands and stacking faults) of 3C-SiC films grown on Si substrates. The measurements revealed a lower resistance of the region containing the defects than of the surrounding area even in the case of layers with high ($5 \cdot 10^{18}$ cm^{-3}) intentional doping concentration. In such a case the current will preferentially flow through these defects.

Therefore, given the high value of unintentional doping in SiC NWs, the use of Schottky barrier (SB) contacts in source and drain is mandatory [72]. Indeed, it has been shown that the drain current modulation is possible (figure 22) by adjusting the transparency of Ti/Au SB through the gate action and in addition, a significant current is flowing through the nanowire only for positive gate voltages. An I_{on}/I_{off} value of 10^3 has been obtained in this case [72], while it was not possible to estimate the transconductance and carrier mobility value by using the above formulas since these are valid only for ohmic contact devices [72]. The SiC NWFETs with ohmic source and drain contacts perform poorly due to the fact that the doping in the nanowire is too high preventing the nanowire of becoming fully depleted in the off-state. If nanowires with reduced doping could be grown then the ohmic contact devices would surely outperform the SB devices (SiC SBNWFETs) by a wide margin.

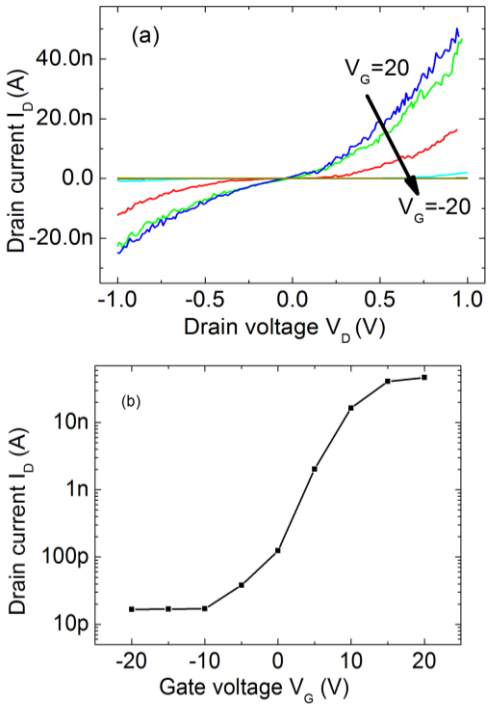

Figure 22. (a) Output and (b) transfer characteristics of a SB-NWFET after RTA; transfer characteristics at V_D=1 V. A Ti/Au scheme was used as Source/Drain metallic pads (Reproduced with permission [72] ©IEEE).

4.2. Field Emission Cathodes

Nanostructures are offering intrinsic advantages for the fabrication of field emitters (FE). In general, for FE applications, a high aspect ratio is highly desirable to obtain a low threshold voltage for emission. In the case of nanowires, this aspect ratio is considerably increased compared to bulk materials. Apart from the geometry of the material, another important parameter is the low electron affinity that permits the emission of electrons for lower applied electric fields and leads to higher emission current density. The low electron affinity, of 3.3 eV [73], provides an extra advantage for SiC compared to Si for FE applications. Moreover, the superior chemical and physical stability of SiC would result to a longer lifetime of the device by minimizing emission instabilities. Therefore, SiC NWs are very promising for FE applications.

Early publications have evidenced good FE properties of SiC nanowires/nanorods [74]. In a later study [7], the field-emitting properties of oriented SiC nanowire arrays were excellent, with a lower turn-on field (0.7-1.5 V/μm), a lower threshold field (2.5-3.5 V/μm), and remarkable electron-emitting stability (24 hr of continuous operation). Excellent stability of SiCNW-based emitters has been also demonstrated in the study of Yang et al. [75]. No obvious degradation of the current density (0.57 mA cm^{-2}) was observed over 1200 min at an applied voltage value of 3000 V. Spanakis et al. [76]

presented results of the attempt to produce arrays of sharp SiC electron emitters by ultraviolet pulsed-laser processing of single-crystal SiC surfaces. This simple one-step technique, has demonstrated efficient SiC cold cathodes that have a lower turn-on field (1.8-2.2 V/μm) than their Si-based counterparts (2.7-3.3 V/μm) and that are able to yield higher current densities at a given operation voltage [76]. Moreover, Kim *et al*. [77] reported the fabrication of, diode-type, field-emission-display (FED) devices with 3C-SiC NWs-based cathodes, which also demonstrated excellent FE properties at low applied voltages/electric fields and stable long-term performance.

SiC nanowires coated with an optimized SiO_2 thickness have higher field emission current than the bare SiC nanowires [41]. Indeed, the wide-bandgap SiO_2 shell layer has small electron affinity (0.6–0.8 eV) and can enhance field emission of SiC emitters. The turn-on field was 4.0 V/μm (bare SiC nanowires), 3.3 V/μm (10 nm SiO_2-coated SiC) and 4.5 V/μm (20 nm SiO_2-coated SiC nanowires) [41]. For very thick shell layer the results get worse quite probably due to a charge build-up at the shell layer–SiC emitter due to limited electron supply through a thick insulating layer.

The density of NWs has also to be optimized to get best field emission properties [40]. The authors concluded that a similar mechanism as in the field emission properties of CNTs holds for SiC NWs. More precisely emission from low-density CNT-films or equivalently SiC NWs, was poor because there were few emitting sites, whereas the emission from densely packed CNT-films was low due to screening effects. In the intermediate regime, the distance between CNTs was sufficient to reach substantial local fields, and the available emitter density was still sufficient for adequate emission currents.

The above reported excellent field-emitting properties of SiC nanowires have usually been characterized in low-voltage fields. However high-voltage fields are often imposed, and intense-current emission is needed in vacuum microelectronics applications, such as high-power microwave tubes and betatrons. Li et al [32] have studied the electron-emitting properties of SiC nanowires in high-voltage electric fields. The emission current approached 118.6 kA, and the current density was calculated to be 23.8 kA/cm^2 when a pulsed high voltage of 109 kV was applied. The corresponding electric field was calculated to be 10.9 V/μm. For comparison, parallel experiments with different cathodes based on a stainless iron wafer, a graphite wafer, and a velvet film were also conducted, and the emission current densities were 4.2, 20.7, and 14.7 kA/cm^2, respectively [32]. Note that velvets are usually employed in the area of intense-current emission at present. However, their emission stabilities are poor because they will be melted and decomposed in a high-voltage electric field, which will decrease the emission current. Thus, SiC nanowires are expected to have great potential applications in the areas of high-microwave-power-tube devices, since they have exhibited higher current density than velvets and in principle SiC has a high melting point and is thermally and chemically stable at high temperature.

5. Conclusions and future prospects

SiC NWs have been grown by a variety of experimental configurations using different growth mechanisms. Each method present specific advantages and it is very difficult to conclude which experimental configuration/growth mechanisms result in the best quality SiC NWs suitable for all applications. The basic differences between the various growth methods are related to the NW dimension, the growth throughput, the use or not of metallic catalyst, the required maximum temperature, the cost of the precursors, the feasibility of preparing radial heterostructures etc.

The VLS-based growth allows high NW growth rate, control of the NWs diameter and length, control of the NW-growth-location and possibility of in-situ doping. The disadvantages of this growth mode deal with the presence of the catalyst having an influence in the NWs properties and the relatively high cost mainly due to the extra step of catalyst-cluster formation. The growth of NWs based on VS mechanism result in high quantities of SiC NWs, free of catalysts at a low cost although there is an inherent difficulty to control the NW-growth-locations and this would impose extra technological steps for integrating the SiC NWs. The SLS mechanism gives more possibilities in controlling the orientation of the NWs and the NW sheath material. The conversion of Si- or C-

containing 1D structures is very promising since it allows a better control of the growth environment and consequently of the SiC NWs, geometry, produced quantity and physical properties. However, it is a high cost method since 1D structures have to be formed prior to the final step of conversion to SiC and it is not optimized up to now.

There is no substantial differences between the growth methods in what it concerns crystalline quality of individual NWs. For all methods there are reported examples of fabricated polycrystalline NWs. Single crystalline nanowires with different densities of planar defects and particularly stacking faults have been grown. It seems that there is no experimental study demonstrating 3C-SiC NWs free of planar defects or at least with a very low density.

6H-SiC NWs could be obtained only in presence of aluminum with the consequence of the high aluminum incorporation in the NWs. This results in a decrease of the lattice constant and the existence of strain in the crystal as well as the presence of strong Al-related luminescence. An extremely high number of twins and stacking faults has been also observed in 6H-SiC NWs probably due to the strain induced by the high Al incorporation.

The influence of quantum confinement in optical properties is questionable despite the observed photoluminescence blue shifts and Raman modes red-shifts. The diameter of the NWs is higher than the atomic Bohr radius but, as in many cases the whole volume of NWs is occupied by SFs with a width lower than 5 nm and thus, quantum confinement could influence the optical properties. However, a systematic study relating the proportion of "fully-stacking-faulty" NWs to the total number as well as the width of SFs with wavelength shift, is missing.

The study of mechanical, thermoelectric and hydrophobic properties of SiC NWs is limited and additional work is necessary towards their complete description, which is necessary for evaluating their potential for related applications.

There is a series of quality criteria with different weight factor for each application. For example, for nanoelectronic applications the carrier concentration and mobility should be accurately controlled along the nanowire. The first experiments on 3C-SiC based NWFETs, revealed that the carrier concentration is too high, due to unintentional doping, resulting in very low electron mobility. Possible causes for this high residual doping values are impurities contamination and/or large number of extended defects. It seems difficult to obtain monocrystalline SiC NWs without extended defects like SFs and low residual doping with the low cost "chemistry-driven" methods used up to now. Relatively high cost methods (Molecular Beam Epitaxy, high-purity CVD, etc.) used in semiconductor device technology should be used towards the aim of fabrication of SiC NWFETs.

For other applications such as mechanical reinforcing these issues of mobility and residual doping are not so critical. Instead of the single crystal production, a high growth method throughput and large length to diameter ratio are demanded. Moreover, for thermoelectric applications, the use of polycrystalline SiC NWs and of high surface roughness could eventually lead to the targeted device performance. The first results related to the use of SiC NWs as reinforcing material are very promising showing a realistic industrial perspective especially for operation at high temperature and/or oxidizing environments.

SiC NWs have exhibited excellent field-emitting properties in both low and high electric fields and are under investigation for related industrial applications like the fabrication of field-emission displays.

Surprisingly there is no any important effort of employing SiC NWs for sensing applications despite the interesting physical properties of SiC material. This is obviously an open area for further exploration.

Acknowledgments

The authors acknowledge Edwige Bano for her contribution to SiC NWFETs development. They are grateful to Jean Camassel, Ioannis Stoemenos, Mikhael Bechelany, Eleftherios Iliopoulos, Emmanouel Spanakis and Katerina Tsagaraki for their critical reading of this paper and/or helpful comments. Finally, the authors thank Professor Patrick Soukiassian for the invitation to write this

review article and arranging the review. K.Z. has been supported by the project NANOTAIL (*Marie Curie Host Fellowship for Transfer of Knowledge*, Contract No. MTKD-CT-2006-042459).

References

[1] Special Issue on Nanowire Transistors: Modeling, Device Design, and Technology 2008 *IEEE Trans. Electron Dev.* **55** 2813-3135
[2] Appenzeller J, Knoch J, Björk M T, Riel H, Schmid H and Riess W 2008 *IEEE Trans. Electron Dev.* **55** 2827-45
[3] Yang P 2005 *MRS Bull*. **30** 85-91
[4] Stern E, Vacic A and Reed M A 2008 *IEEE Trans. Electron Dev.* **55** 3119-30
[5] Special Issue on Silicon Carbide Devices and Technology 2008 *IEEE Trans. Electron Dev.* **55** 1795-2065
[6] Seong H K, Choi H J, Lee S K, Lee J I, Choi D J 2004 *Appl. Phys. Lett.* **85** 1256 and in Seong H K, Choi H J, Lee S K, Lee J I and Choi D J 2006 *Mater. Sci. Forum* **527–529** 771-75
[7] Pan Z W, Lai H L, Frederick C K, Duan X F, Zhou W Y, Shi W S, Wang N, Lee C S, Wong N B, Lee S T and Xie S S 2000 *Adv. Mater.* **12** 1186
[8] Niu J J, Wang J N, Xu Q F 2008 *Langmuir* **24** 6918
[9] Wong E W, Sheehan P E, Lieber C M, 1997 *Science* **277** 1971
[10] *The International Technology Roadmap for Semiconductors (ITRS): 2009 Emerging Research Devices* http://www.itrs.net/reports.html p 28
[11] Li Y, Kish L B 2006 *Fluctuations & Noise Lett.* **6** L127-31
[12] Kim D W, Choi Y-C, Choi K-J, Park J-G, Park J H, Pimenov S M, Frolov V D, Abanshin N P, Gorfinkel B I, Rossukanyi N M and Rukovishnikov A I 2008 *Nanotechnology* **19** 225706
[13] Wang X H , Eguchi K, Iwamoto C and Yoshida T 2003 *Science and Technology of Advanced Materials* **4** 167–72
[14] Papanikolaou N 2008 *J. Phys.: Condens. Matter* **20** 135201
[15] Kimoto T. Itoh A and Matsunami H 1997 *Phys. Stat. Sol (b)* **202** 247-62
[16] Hollar W E and Kim J J 1991 *Ceram. Eng. Sci. Proc*. **12** 979
[17] Janeuay P. A. 1992 *Ceram. Ind.* **4** 42
[18] Zhou D and Seraphin S 1994 *Chem. Phys. Lett*. **222** 233
[19] Dai H, Wong E W, Lu Y Z, Fan S and Lieber CM 1995 *Nature* (London) **375** 769-72
[20] Li C P, Fitzgerlad J D, Zou J and Chen Y 2007 *New Journal of Physics* **9** 137
[21] Ye H, Titchenal N, Gogotsi Y and Ko F 2005 *Adv. Mater.* **17** 1531-35
[22] Zhou W M, Fang F, Hou Z Y, Yan L J, and Zhang Y F 2006 *IEEE Electron Dev. Lett.* **27** 463-65
[23] Zekentes K, Papaioannou V, Pecz B and Stoemenos J 1995 *J. Cryst. Growth* **57** 392-99
[24] Zekentes K, Becourt N, Androulidaki M, Tsagaraki K, Stoemenos J, Bluet J M, Camassel J and Pascual J 1996 *Appl. Surf. Sci.* **102** 22
[25] Zhang Y F, Tang Y H, Zhang Y, Lee C S, Bello I and Lee S T 2000 *Chem. Phys. Lett.* **330** 48-52
[26] Tsakalakos L, Fronheiser J, Rowland L, Rahmane M, Larsen M, and Gao Y 2007 *Mater. Res. Soc. Symp. Proc.* **963** 0963-Q11-03
[27] Ollivier M, Mantoux A, Bano E, Rogdakis K, Zekentes K, Baron T and Latu-Romain L accepted in *Mat. Sci. Forum.*
[28] Zhou X T, Wang N, Lai H L, Peng H Y, Bello I , Wong N B, Lee C S, and Lee S T 1999 *Appl. Phys. Lett*. **74** 3942-45
[29] Fortuna S A and Li X 2010 *Semicond. Sci. Technol.* **25** 024005
[30] Wagner R S and Ellis W C 1964 *Appl. Phys. Lett.* **4** 89–90
[31] Choi H J, Seong H K, Lee J C, Sung Y M 2004 *J. Cryst. Growth* **269** 472–478
[32] Li G Y, Li, X D, Chen Z D, Wang J, Wang H and Che R C 2009 *J. Phys. Chem. C* **113** 17655–60
[33] Colli A, Hofmann S, Fasoli A, Ferrari A C, Ducati C, Dunin-Borkowski R E and Robertson J 2006 *Appl. Phys. A* **85** 247–53

[34] Zhang H, Ding W Q, He K and Li M 2010 *Nanoscale Res Lett* **5** 1264
[35] Bechelany M, Cornu D, 2006, *World Patent* WO2006/067 308 and Bechelamy M, Brioude A, Stadelmann P, Ferro G, Cornu D and Miele P 2007, *Adv. Funct. Mater.* **17** 3251-57
[36] Wu R, Li B, Gao M X, Chen J J, Zhu Q M, Pan Y 2008 *Nanotechnology* **19** 335602
[37] Ju Z C, Xing Z, Guo C L, Yang L, Xu L and Qian Y 2008 *Eur. J. Inorganic Chem.* **24** 3883–88
[38] Lu Q Y, Hu J Q, Tang K B, Qian Y T, Zhou G, Liu X and Zhu J S 1999 *Appl. Phys. Lett*. **75** 507
[39] Xing Y J, Hang Q L, Yan H F, Pan H Y, Xu J, Yu D P, Xi Z H, Xue Z Q, Feng S Q 2001 *Chem. Phys. Lett.* **345** 29-32
[40] Yang T.H. Chen C H, Chatterjee A, Li H Y, Lo J T, Wu C T, Chen K H and Chen L C 2003 *Chem. Phys. Lett.* **379** 155–61
[41] Ryu Y, Tak Y and Yong K 2005 *Nanotechnology* **16** S370–74
[42] Li Y B, Xie S S, Zhou W Y, Ci L J and Bando Y 2002 *Chem. Phys. Lett.* **356** 325
[43] Gao F M, Yang W Y, Wang H T, Fan Y, Xie Z P and An L A 2008 *Cryst. Growth Des.* **8** 1461
[44] Wei G, Qin W, Wang G, Sun J, Lin J, Kim R, Zhang D and Zheng K 2008 *J. Phys. D: Appl. Phys.* **41** 235102
[45] Li F and Wen G 2007 *J. Mater. Sci.* **42** 4125-30
[46] Li Z J, Li X J, Chen X L, Meng A L, Li K L, Xu Y P and Dai L 2003 *Appl. Phys. A* **76** 637–40
[47] Mahadik N, Qadri S B, Sundaresan S G, Rao M V, Tian Y L and Zhang Q C 2009 *Surf. & Coat. Technol.* **203** 2625–27
[48] Polychroniadis E, Syväjärvi M, Yakimova R and Stoemenos J 2004 *J. Crys. Growth* **263** 68
[49] Bechelany M, Brioude A, Cornu D, Ferro G and Miele P 2007 *Adv. Funct. Mater.* **17** 939
[50] Shen G Z, Bando Y, Ye C H, Liu B D and Golberg D 2006 *Nanotechnology* **17** 3468–3472
[51] Richter H, Wang Z P, Ley L 1981 *Sol. St. Communications*, **39** 625-9
[52] Wu X L, Fan J Y, Qiu T, Yang X, Siu G G and Chu P K 2005 *Phys. Rev. Lett.* **94** 026102
[53] Niu J J and Wang J N 2007 *J.* Phys. *Chem. B* **111** 4368
[54] Li Z J, Zhang J L, Meng A and Guo J Z 2006 *J. Phys. Chem. B* **110** 22382-86
[55] Hu J Q, Lu Q Y, Tang K B, Deng B, Jiang R R, Qian Y T, Yu W C, Zhou G E, Liu X M and Wu J X 2000 *J. Phys. Chem. B* **104** 5251
[56] Hirano R, Tajima M and Itoh K M 2010 *Mat. Sci. Forum*. **645-648** 355-8
[57] Hu J Q, Bando Y, Zhan J H and Golberg D 2004 *Appl. Phys. Lett.* **85** 2932
[58] Zhang L G, Yang W Y, Jin H, Zheng Z H, Xie Z P, Miao H Z and An L N 2006 *Appl. Phys. Lett.* **89** 143101
[59] Rossi A M, Murphy T E and Reipa V 2008 *Appl. Phys. Lett.* **92** 253112
[60] Yang W, Araki H, Tang C C, Thaveethavorn S, Hiroshi A K and Noda T 2005 *Adv. Mater.* **17** 1519
[61] Han X D, Zhang Y F, Zheng K, Zhang X N, Zhang Z, Hao Y J, Guo X Y, Yuan J and Wang Z L 2007 *Nano Lett.* **7** 452
[62] Perisanu S, Gouttenoire V, Vincent P, Ayari A, Choueib M, Bechelany M, Cornu D, Purcell ST 2008 *Phys. Rev. B* **77** 165434
[63] Pensl G, Ciobanu F, Frank T, Krieger M, Reshanov S, Schmid F and Weidner M 2005 *Int. J. High-Speed Electronics & Systems* **15** 705-745
[64] Wagner C and Krötz G 1997 *Diam. Rel. Mat.* **6** 1338-41
[65] Takahashi K, Ito Y, Ikuta T, Nishiyama T, Fujii M, Zhang X and Huczko A 2008 *HighTemp.—HighPress.* **37** 119–25
[66] Lee K M, Choi T Y, Lee S K and Poulikakos D 2010 *Nanotechnology* **21** 125301
[67] Rogdakis K, Lee S Y, Bescond M, Lee S K, Bano E and Zekentes K 2008 *IEEE Trans on Elec. Dev.* **55** 1970
[68] Rogdakis K, Bescond M, Bano E and Zekentes K 2007 *Nanotechnology* **18** 475 715 and in Rogdakis K, Bescond M, Zekentes K and Bano E 2009 *Mat. Sci. Forum.* **600-603** 579-82
[69] Rogdakis K, Poli S, Bano E, Zekentes K and Pala M 2009 *Nanotechnology* **20** 295202

[70] Jang C O, Kim T H, Lee S Y, Kim D J and Lee S K 2008 *Nanotechnology* **19** 345203
[71] Song X, Michaud J F, Cayrel F, Zielinski M, Portail M, Chassagne T, Collard E and Alquier D 2010 *Appl. Phys. Lett.* **96** 142104
[72] Rogdakis K, Lee S Y, Kim D J, Lee S K, Bano E and Zekentes K 2009 *Mat. Sci. Forum* **615-617** 235-238 and in Rogdakis K, Bano E, Montes L, Bechelany M, Cornu D and Zekentes K accepted in *IEEE Trans. on Nanotechnology*
[73] Wiets M, Weinelt M, and Fauster T 2003 *Phys. Rev. B* **68** 125321
[74] Chen H, Yin Y Z and He Y J 2000 *Mod. Phys. Lett.* ***B*** **14** 131–8
[75] Yang Y J, Meng G W, Xianyun Liu, Lide Zhang, Zheng Hu, Chengyu He, and Yemin Hu J. Phys. Chem. C, Vol. 112, No. 51, 2008 20126
[76] Spanakis E, Dialektos J, Stratakis E, Zorba V, Tzanetakis P and Fotakis C 2008 *Phys. Stat. Sol. C* **5** 3309-13
[77] Kim D W, Choi Y J, Choi K J, Park J G, Park J H, Pimenov S M, Frolov V D, Abanshin N P, Gorfinkel B I, Rossukanyi N M and Rukovishnikov A I 2008 *Nanotechnology* **19** 225706